Article

Discovery Medicine 2024; 36(190): 2231–2243
https://doi.org/10.24976/Discov.Med.202436190.205

Propofol Triggers Cell Death in Lung Cancer Cells by Increasing PANX1 Expression, Activating the Mitochondrial Cell Death Pathway, and Enhancing ROS Levels

Jie Zhang[1], Anqing Chen[2], Yonggang Song[3,*]

[1]Department of Anesthesiology, Yantaishan Hospital, 264000 Yantai, Shandong, China
[2]Laboratory Department, Qingdao Hospital, University of Health and Rehabilitation Sciences (Qingdao Municipal Hospital), 266000 Qingdao, Shandong, China
[3]Anesthesiology and Perioperative Medicine Department, Shandong Public Health Clinical Center, 250000 Jinan, Shandong, China
*Correspondence: 13864096775@163.com (Yonggang Song)
Published: 20 November 2024

Background: Lung cancer treatment remains a global challenge due to tumor cell resistance. Propofol, traditionally used as an anesthetic, has demonstrated potential anti-tumor properties. This study seeks to elucidate how propofol induces cell death in lung cancer cells by upregulating Pannexin 1 (PANX1) expression, activating the mitochondrial cell death pathway, and augmenting reactive oxygen species (ROS) production.

Methods: In this study, the A549 lung cancer cell line was employed as the experimental model. Cells underwent exposure to varying propofol concentrations and were pre-treated with H_2O_2 and N-acetylcysteine (NAC) to simulate oxidative stress and antioxidant conditions. Various techniques, including 5-Ethynyl-2′-deoxyuridine (EdU), colony formation, Transwell, 2′,7′-Dichlorodihydrofluorescein diacetate (DCFH-DA), Terminal deoxynucleotidyl transferase dUTP Nick End Labeling (TUNEL), and JC-1 (5,5′,6,6′-Tetrachloro-1,1′,3,3′-tetraethyl-imidacarbocyanine iodide) probes, were employed to evaluate propofol's effects on lung cancer cell viability, growth, invasion, ROS levels, apoptosis, and mitochondrial membrane potential. Western blot analysis was used to measure PANX1, B-cell lymphoma 2 (Bcl-2), Bcl-2-associated X protein (Bax), caspase-3, and Cytochrome C (Cyt C) protein levels. Additionally, PANX1's influence on propofol-induced apoptosis was investigated through siRNA interference.

Results: The experiment unveiled propofol's dose-dependent inhibition of A549 lung cancer cell growth, coupled with decreased cell proliferation and invasion attributable to heightened ROS production. Notably, propofol treatment significantly elevated mitochondrial membrane potential, signifying activation of the mitochondrial cell death pathway ($p < 0.01$). Furthermore, propofol upregulated PANX1 expression ($p < 0.01$), thereby intensifying apoptosis signaling, whereas PANX1 inhibition ameliorated propofol-induced apoptosis ($p < 0.01$). These findings underscore the pivotal role of PANX1 upregulation and ROS augmentation in propofol-induced apoptosis in lung cancer cells.

Conclusion: This study provides evidence that propofol induces cell death in lung cancer cells by upregulating PANX1, activating the mitochondrial apoptosis pathway, and increasing ROS production. These findings suggest that targeting PANX1 and ROS could enhance the anti-cancer efficacy of propofol in lung cancer.

Keywords: lung cancer; propofol; PANX1; mitochondrial apoptosis; ROS

Introduction

Lung cancer, ranking among the malignancies with the highest mortality rate globally, continues to pose significant challenges with persistently high incidence and mortality rates [1,2]. Despite notable advancements in treatment modalities over recent years—including surgery, radiation, chemotherapy, and targeted therapy—the five-year survival rate for patients remains disheartening due to low rates of early detection and limited treatment efficacy [3,4]. Consequently, the exploration of novel treatment strategies, particularly for patients with advanced lung cancer, has emerged as a crucial focus in current lung cancer research [2,5–10].

The conventional treatment approaches for lung cancer primarily encompass surgery, chemotherapy, radiotherapy, and targeted therapy. Surgery stands as the primary treatment for early-stage lung cancer, particularly for tumors amenable to local resection. Chemotherapy and radiotherapy typically serve advanced-stage lung cancer patients or those unsuitable for surgical resection, aiming to alleviate symptoms, extend survival, or reduce tumor bur-

Copyright: © 2024 The Author(s). Published by Discovery Medicine. This is an open access article under the CC BY 4.0 license.
Note: *Discovery Medicine* stays neutral with regard to jurisdictional claims in published maps and institutional affiliations.

den. Targeted therapy entails treatment directed at specific molecular targets in lung cancer, such as epidermal growth factor receptor (EGFR) mutations and anaplastic lymphoma kinase (ALK) fusion genes. These targeted therapy agents can enhance treatment outcomes for patients harboring these mutations.

However, these conventional treatment modalities exhibit certain limitations. Surgery may not be feasible for advanced-stage lung cancer patients, and post-surgical recurrence rates are relatively high. The toxic side effects associated with chemotherapy and radiotherapy may diminish patients' quality of life, and some tumors may develop resistance to these treatments. Targeted therapy is only applicable to patients with specific genetic mutations, and resistance or other escape mechanisms may arise over time.

Recent research highlighted the significance of Pannexin 1 (PANX1), a protein located in cell membranes, in regulating cell death, inflammation, and tumor growth [11,12]. Specifically, during the apoptosis process of tumor cells, the upregulation of PANX1 can facilitate the transmission of apoptosis signals, thereby expediting the demise of tumor cells [13–15]. The mitochondrial pathway for cell death constitutes a pivotal process that triggers apoptosis by releasing Cytochrome C, activating caspase proteins, and employing other mechanisms. Reactive oxygen species (ROS), acting as crucial signaling molecules, play a pivotal role in the mitochondrial pathway of apoptosis [16–18]. Excessive ROS accumulation can induce oxidative stress in the intracellular environment, thereby instigating the mitochondrial apoptosis pathway and culminating in cell death [19,20].

Propofol, a widely utilized intravenous anesthetic renowned for its rapid and short-acting effects, finds extensive application in clinical settings [21]. Recent investigations have indicated that beyond its anesthetic properties, propofol may also exert influence over the growth and demise of cancer cells through diverse pathways [22–24]. However, the mechanism by which propofol induces cancer cell death, specifically through increased PANX1 expression, activation of the mitochondrial apoptosis pathway, and augmentation of ROS generation, remains largely unexplored among these pathways. Further research and validation are imperative to delve into the impact of propofol on the proliferation and demise of lung cancer cells, along with its potential clinical applications.

The aim of this research is to investigate the mechanisms through which propofol induces cell death in lung cancer cells by enhancing PANX1 expression, activating the mitochondrial cell death pathway, and increasing ROS generation. This study will assess the impact of propofol on lung cancer cell growth and apoptosis, as well as its role in modulating PANX1 expression and influencing ROS levels via the mitochondrial apoptosis pathway using *in vitro* cell experiments and molecular biology techniques. The findings of this research will not only offer a fresh perspective on propofol's anti-tumor mechanism but also provide a theoretical basis and experimental evidence for the utilization of propofol in lung cancer treatment, holding significant scientific importance and promising clinical implications.

Materials and Methods

Cell Culture and Transfection

A549 cells (CL-0016), procured from Wuhan Puno Sai Life Technology Co., Ltd. (Wuhan, China), were revived and cultured in DMEM medium supplemented with 10% fetal bovine serum (iCell-0500, iCELL, Shanghai, China) and 1% penicillin-streptomycin (iCell-15140-122, iCELL, Shanghai, China). The cells were maintained in a constant temperature incubator at 37 °C with 5% CO_2. DMEM was supplied by Gibco (MT15017CV, Wilmington, MA, USA).

The cells were divided into Control, Propofol (25 µmol/L) (YZ-100806, China National Institutes for Drug Control, Beijing, China), Propofol+N-acetylcysteine (NAC) (5 mmol) (SA5830, Solarbio, Beijing, China), and Propofol+H_2O_2 (60 mmol) groups for various intervention treatments. Cells were passaged and plated once they reached 80% to 90% confluence. A549 cells in the rapid growth phase were treated with trypsin and then seeded onto culture dishes. Cells were transfected when they reached a confluence of 50% to 70%.

For transfection, siRNA and Lipofectamine 2000 (11668-019, Invitrogen, Wilmington, MA, USA) were separately incubated with DMEM for 5 minutes. Subsequently, the two components were combined and allowed to incubate for an additional 20 minutes. The resulting mixture was then introduced into the cell culture dishes.

Two groups were established: the Negative control group (NC group) and the silenced group (siRNA *PANX1* group), each comprising three replicates. SiRNA *PANX1* was synthesized by Beijing Hesheng Biotechnology Co., Ltd. (Beijing, China). The sequences were as follows: SiRNA-NC (sense: 5′-UUCUCCGAACGUGUCACGUTT-3′, antisense: 5′-ACGUGACACGUUCGGAGAATT-3′); SiRNA-*PANX1* (sense: 5′-GAGAGAGUUUGAAAUUAUATT-3′, antisense: 5′-UAUAAUUUCAAACUCUCUCTT-3′).

Following transfection for 4 to 6 hours, the DMEM was replaced with 10% fetal bovine serum. Following transfection for 48 hours, cell proteins were extracted according to the instructions to verify the efficiency of transfection. All cell lines employed in this study underwent STR authentication and mycoplasma screening.

CCK-8 Assay

A549 cells (1×10^5 cells/well) in the rapid growth stage were detached using trypsin and seeded into a 96-well dish, with three duplicates for each set. The cells were then incubated in a stable environment at 37 °C with 5%

CO_2. Subsequently, Cell Counting Kit-8 (CCK-8) (C0037) reagent obtained from Beyotime Institute of Biotechnology (Shanghai, China) was added to the culture, followed by a 2-hour incubation period. The absorbance of each well was measured at 450 nm using a microplate reader (SpectraMax iD3, Molecular Devices, San Jose, CA, USA), and the resulting OD values were analyzed to assess cell proliferation.

EdU Assay

Cells (1×10^5 cells/well) in the exponential growth phase from all groups were seeded onto 24-well cell culture inserts. Once the cells adhered to the surface, 300 microliters of 5-Ethynyl-2′-deoxyuridine (EdU) solution (50 micromoles per liter) was added to each well and allowed to incubate for 2 hours. The EdU-488 Cell Proliferation Assay Kit (C0071S) by BeyoClick™ was procured from Shanghai Beyotime Biotechnology Co., Ltd. (Shanghai, China).

Following the incubation, the cells were fixed using 4% paraformaldehyde at room temperature for 30 minutes and then treated with 0.5% Triton X-100 in PBS for 10 minutes. Apollo staining solution was applied, followed by incubation on a shaker in darkness at room temperature for 30 minutes. Subsequently, DNA staining was performed using 4′,6-diamidino-2-phenylindole (DAPI) staining solution. After the staining procedure, cells were observed under a microscope (IX83, Olympus, Tokyo, Japan), and five random fields of view were selected for cell counting. The EdU-positive cell rate in each group of A549 cells was then calculated.

Transwell Assay

Cell migration assay: add cell suspension containing appropriate culture medium to the upper chamber of the Transwell plate, and add the same culture medium or medium containing sufficient chemoattractants to induce cell migration to the lower chamber. Add the cell suspension to the upper chamber of the Transwell plate. Place the plate in a cell culture incubator for a period of time to allow cell migration through the pores of the plate. Remove non-migrated cells from the upper chamber, fix and stain migrated cells. Use a microscope (CX83, Olympus, Tokyo, Japan) to observe and capture images of migrated cells, and perform quantitative analysis of the images.

Cell invasion assay: coat the upper chamber of the Transwell plate with a layer of ECM (extracellular matrix) or matrix (such as Matrigel) to mimic cell invasion under physiological conditions. Add the cell suspension to the upper chamber of the Transwell plate. Place the plate in a cell culture incubator for a period of time to allow cell invasion through the ECM or matrix layer. Remove non-invading cells from the upper chamber, fix and stain the invading cells. Use a microscope (CX83, Olympus, Tokyo, Japan) to observe and capture images of the invading cells, and perform quantitative analysis of the images. Quantitative analysis of images was performed using Image J software (version 1.48, National Institutes of Health, Rockville, MD, USA).

Cell Colony Formation Assay

A549 cells (500 cells/well) were evenly distributed into 6-well dishes, with each group containing three replicates. Once colonies were established, the medium was aspirated, and the cells were treated with 4% paraformaldehyde, followed by incubation for 30 minutes in each well. Subsequently, the cells were stained with 0.1% crystal violet for 20 minutes and left to dry. Finally, photographs of the stained colonies were captured using a digital camera (D850, Nikon, Tokyo, Japan).

TUNEL Assay for Cell Apoptosis

Following the guidelines of the Terminal deoxynucleotidyl transferase dUTP Nick End Labeling (TUNEL) fluorescence kit, reagent 1 (TdT) and reagent 2 (dUTP) were combined in a 1:9 ratio and then applied to the cellular slides. The TUNEL apoptosis detection kit from Roche, Basel, Switzerland (batch number 11684817910), was utilized. The slides were positioned in a chamber with high humidity and maintained at a temperature of 37 °C for 2 hours. Subsequently, 3% bovine serum albumin (BSA) (A8010, Solarbio, Beijing, China) was introduced for room temperature blocking, with a duration of 30 minutes. The primary antibody was incubated overnight in a humid chamber at 4 °C. Afterward, the secondary antibody was incubated in darkness at room temperature for 50 minutes, followed by DAPI staining in darkness at room temperature for 10 minutes. The slides underwent three rinses with PBS for 5 minutes each, then were sealed with anti-fade mounting solution. Pictures were captured using a fluorescent microscope (Eclipse Ti2, Nikon, Tokyo, Japan). Normal cell nuclei stained with DAPI emitted blue fluorescence under UV excitation, while apoptotic cells appeared green.

DCFH-DA Fluorescent Probe Method for Detecting Cellular ROS Levels

Logarithmically growing cells (1×10^5 cells/well) were seeded into 6-well plates. Upon reaching 80% to 90% confluence, cells were subjected to drug treatment under predetermined conditions for 24 hours. Following the removal of the supernatant, cells were gently washed twice with PBS. Subsequently, the 2′,7′-Dichlorodihydrofluorescein diacetate (DCFH-DA) probe was added and allowed to incubate for 30 minutes. The ROS detection kit (lot number 10324010104) was procured from Dingguo Changsheng Biotechnology in Beijing, China. Images were captured using a fluorescence microscope (Eclipse Ti2, Nikon, Tokyo, Japan), with the intensity of green fluorescence serving as an indicator of ROS levels within the cells.

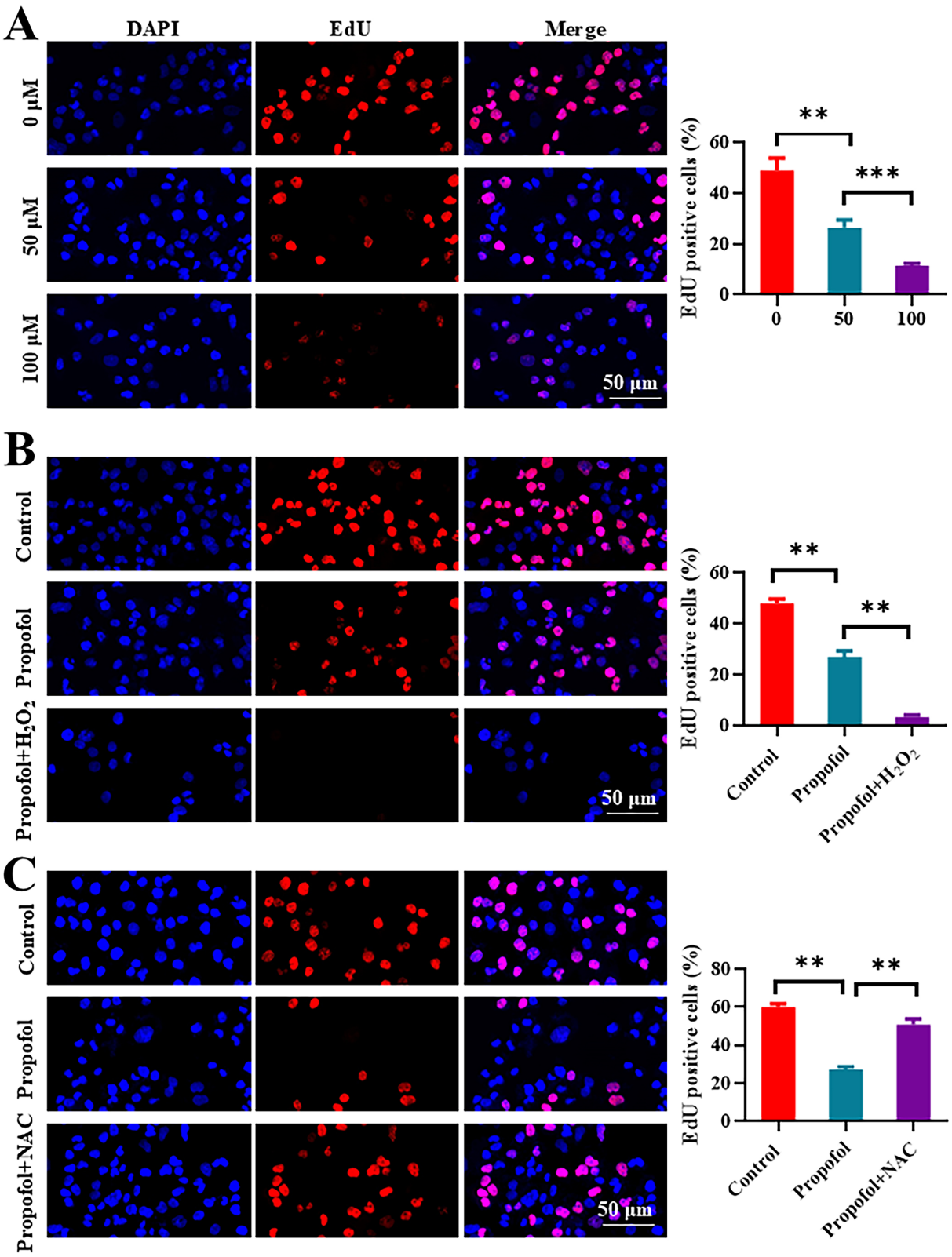

Fig. 1. Propofol inhibits the viability of lung cancer cells. (A) Propofol reduces the growth of A549 lung cancer cells in a manner that depends on the dosage. (B) Pretreatment with H_2O_2 enhances the inhibitory effect of propofol on the viability of A549 lung cancer cells. (C) Pretreatment with N-acetylcysteine (NAC) reduces the inhibitory effect of propofol on the viability of A549 lung cancer cells. N = 6. $^{**}p < 0.01$, $^{***}p < 0.001$. EdU, 5-Ethynyl-2′-deoxyuridine.

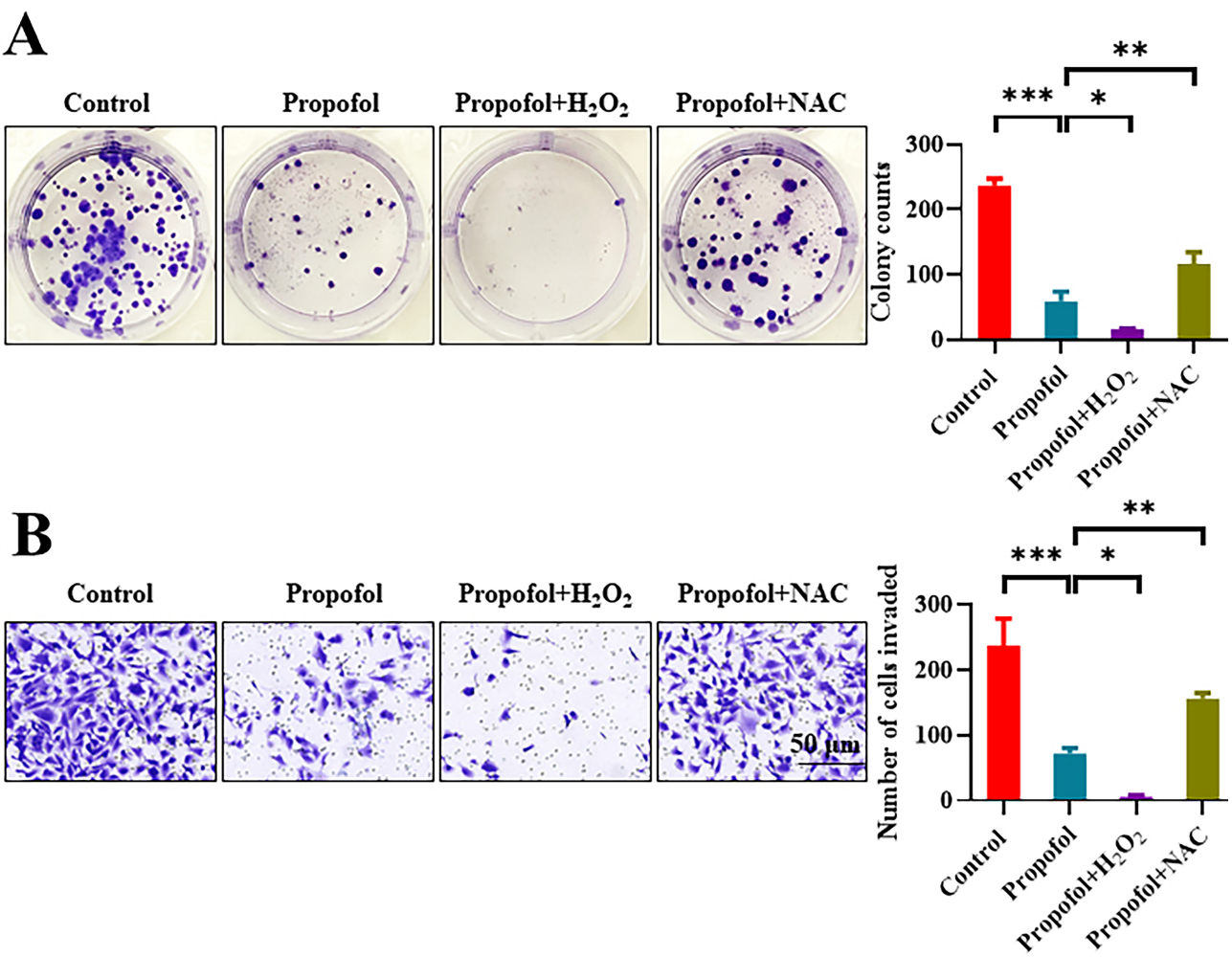

Fig. 2. Propofol inhibits the proliferation and invasion of lung cancer cells by increasing cellular oxidative stress. (A) The effect of different treatments on the clonogenic ability of lung cancer A549 cells was assessed by colony counting. (B) The impact of different treatments on the invasive capacity of lung cancer A549 cells evaluated by transwell assay. N = 6. *$p < 0.05$, **$p < 0.01$, ***$p < 0.001$.

JC-1 Fluorescent Probe Method for Detecting Mitochondrial Membrane Potential

A549 cells (1×10^5 cells/well) were seeded into 6-well dishes according to their respective groups and incubated for 24 hours prior to the removal of the culture medium. Following this, cells were washed with 1 mL of PBS. Each well was then incubated with 1 mL of JC-1 (5,5′,6,6′-Tetrachloro-1,1′,3,3′-tetraethylimidacarbocyanine iodide) staining working solution for 20 minutes. After discarding the supernatant, the cells underwent two washes with JC-1 buffer solution, followed by the addition of 2 mL of culture medium. The mitochondrial membrane potential JC-1 assay kit (batch number: 032421220215) was obtained from Solarbio Science & Technology, Beijing, China. The assessment of membrane potential was conducted by observing the ratio of red to green fluorescence under a fluorescence microscope (IX83, Olympus, Tokyo, Japan).

Western Blot

In each well of a 6-well plate containing cells, 200 µL of cell lysis buffer (RIPA:PMSF = 100:1) from Solarbio Science & Technology, Beijing, China, was added. Following the manufacturer's guidelines, total protein extraction from the cells was performed, and the protein concentration for each group was determined. Subsequently, 20 µg of each protein sample underwent sodium dodecyl sulfate polyacrylamide gel electrophoresis (SDS-PAGE) electrophoresis. The separated proteins were then transferred from the gel onto a nitrocellulose membrane.

For membrane blocking, the membrane was incubated with BSA blocking solution at room temperature for 3 hours. After blocking, the excess blocking solution was removed with filter paper. Primary antibodies (PANX1 (1:1000 dilution, ab124131, Abcam, Cambridge, UK), Bcl-2-associated X protein (Bax) (1:1000 dilution, ab32503, Abcam, Cambridge, UK), B-cell lymphoma 2 (Bcl-2) (1:1000 dilution, ab182858, Abcam, Cambridge,

UK), Cleaved caspase-3 (1:1000 dilution, ab24042, Abcam, Cambridge, UK), Cytochrome C (Cyt C) (1:1000 dilution, ab133504, Abcam, Cambridge, UK), Glyceraldehyde 3-phosphate dehydrogenase (GAPDH) (1:1000 dilution, ab9485, Abcam, Cambridge, UK)) were added with blocking solution and left to incubate overnight at 4 °C.

Following primary antibody incubation, the membrane underwent three washes with Tris-Buffered Saline Tween (TBST) buffer, each lasting 15 minutes. Subsequently, the membrane was incubated with the corresponding secondary antibodies (diluted 1:1000 with blocking solution) at room temperature for 2 hours. Horseradish peroxidase-conjugated secondary antibodies (1:1000 dilution) for mouse and rabbit detection were supplied by Zhongshan Golden Bridge Biotechnology (Beijing, China).

After secondary antibody incubation, the membrane was washed three times with TBST buffer for 15 minutes each. Following this, chemiluminescent substrate was added, and the membrane was imaged using a chemiluminescence imaging system (Tanon-5200, Tanon Science & Technology, Shanghai) for data analysis.

Statistical Analysis

The statistical analysis was performed using the SPSS statistical program (version 25.0, IBM, Armonk, NY, USA). Quantitative data are presented as mean ± standard deviation. One-way analysis of variance (ANOVA) was employed to compare multiple groups, followed by post-hoc tests using Tukey's method for pairwise comparisons. The *t*-test was utilized for comparisons between pairs. A *p*-value less than 0.05 was considered statistically significant.

Results

Propofol Inhibits the Viability of Lung Cancer Cells

The experiment was divided into three main parts to investigate the effects of propofol on the viability of A549 cells, along with the effects of pretreatment with H_2O_2 and NAC on propofol's action. The findings regarding propofol's impact on the survival of A549 lung cancer cells revealed its ability to decrease cell viability in a dose-dependent manner. Specifically, as propofol concentration increased (from 0 μM to 50 μM and then to 100 μM), there was a significant decrease in the EdU positivity rate, indicating reduced cell proliferation ability ($p < 0.01$). This suggests propofol's potential to effectively suppress lung cancer cell growth (Fig. 1A).

Moreover, when A549 cells were pretreated with H_2O_2 before propofol addition, the EdU positivity rate further decreased ($p < 0.01$), more significantly than with propofol alone (Fig. 1B). This indicates that H_2O_2 pretreatment enhances propofol's inhibitory effect on lung cancer cell viability, possibly by elevating intracellular oxidative stress levels, rendering cells more sensitive to propofol.

Conversely, pretreatment with NAC before propofol addition resulted in an increased EdU positivity rate compared to propofol alone, indicating a reduction in propofol's inhibitory effect on lung cancer cell viability ($p < 0.01$) (Fig. 1C). This may be attributed to NAC's ability to reduce intracellular oxidative stress, thereby mitigating propofol-induced apoptosis.

Propofol Suppresses the Growth and Spread of Lung Cancer Cells by Enhancing Cellular Oxidation

The results of the colony formation assay revealed that the control group (Ctrl) exhibited the highest number of lung cancer A549 cell colonies, indicating robust proliferation ability in the absence of treatment. Upon treatment with propofol (propofol group), the number of colonies formed decreased ($p < 0.001$), suggesting propofol's ability to inhibit lung cancer cell proliferation. Notably, the propofol+H_2O_2 group displayed the lowest colony formation ($p < 0.05$), indicating that H_2O_2 enhances propofol's inhibitory effect. Conversely, the propofol+NAC group showed fewer colonies compared to the control group but more than the propofol group ($p < 0.01$), suggesting NAC partially reduces propofol's inhibitory impact (Fig. 2A).

Similarly, the results of the invasion assay mirrored those of the colony formation assay. The number of invading cells decreased in the propofol treatment group ($p < 0.001$), indicating propofol's inhibition of lung cancer cell invasion. Furthermore, the propofol+H_2O_2 group exhibited a further reduction in invading cells ($p < 0.05$), suggesting enhanced inhibition by H_2O_2. Conversely, although the number of invading cells in the propofol+NAC group was lower than in the control group, it was higher than in the propofol group ($p < 0.01$), indicating that NAC weakens propofol's inhibitory effect to some extent (Fig. 2B).

Propofol Treatment Increased the Levels of ROS in A549 Cells, thereby Promoting Cell Apoptosis

ROS levels play a crucial role in apoptosis signaling, and the detection of ROS generation within cells is commonly achieved through DCFH-DA incubation. This study aimed to investigate the impact of propofol and its combination with H_2O_2 and NAC on ROS levels in A549 lung cancer cells using the DCFH-DA incubation technique.

A549 cells treated solely with propofol exhibited increased ROS fluorescence intensity compared to the control group ($p < 0.01$), indicating propofol's ability to elevate ROS levels in cells. When propofol was combined with H_2O_2, the ROS fluorescence intensity further increased ($p < 0.001$), reaching the highest level. This suggests that H_2O_2 enhances propofol-induced ROS upregulation, potentially by exacerbating intracellular oxidative stress and promoting apoptosis. In contrast, the ROS fluorescence intensity decreased when propofol was combined with NAC ($p < 0.05$), although it remained higher than the control group. This indicates that NAC, as an antioxidant, partially

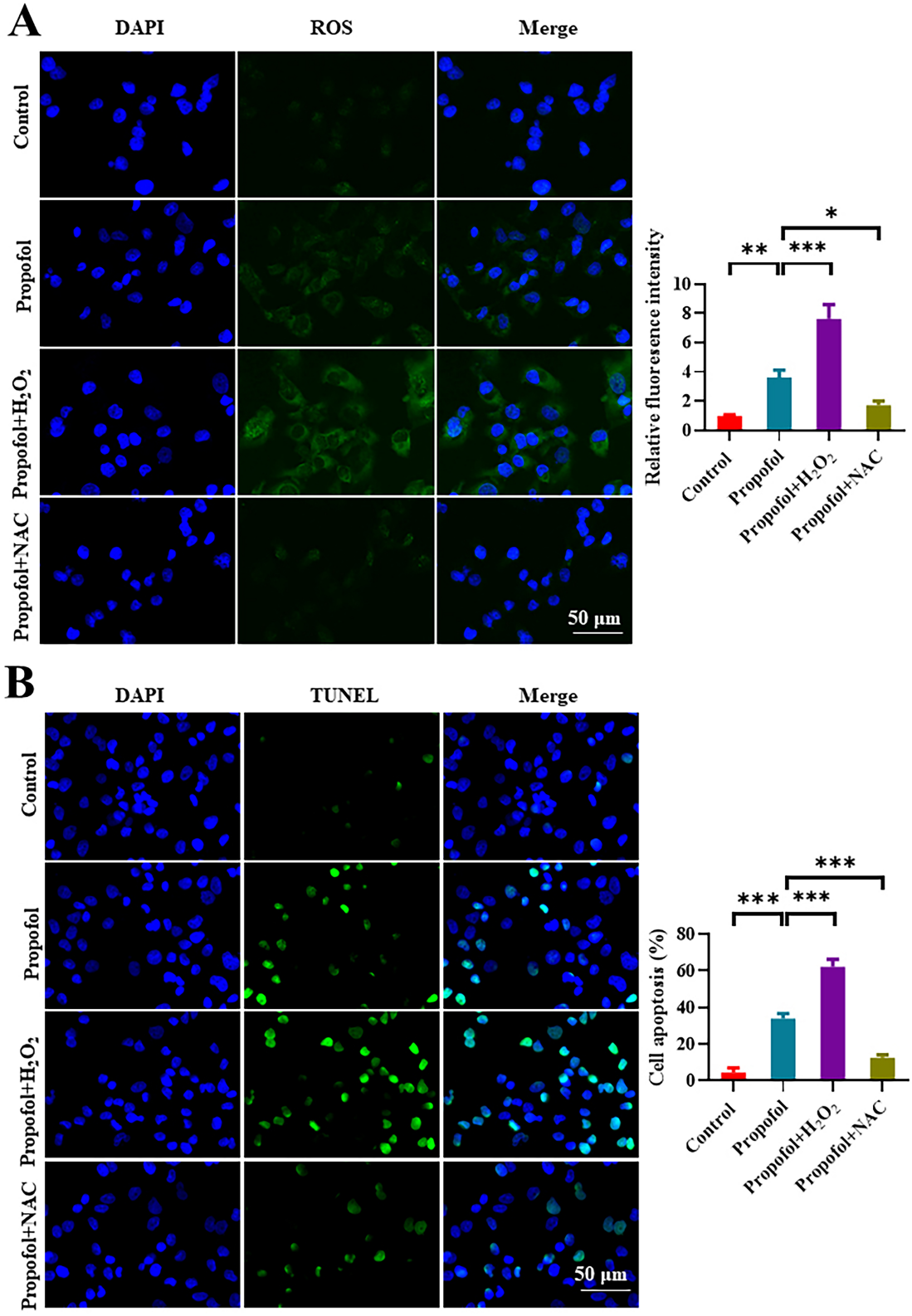

Fig. 3. Levels of reactive oxygen species (ROS) and apoptosis in A549 cells treated with propofol, propofol+H_2O_2, and propofol+NAC. (A) Intracellular ROS generation was analyzed by incubating A549 cells with 2′,7′-Dichlorodihydrofluorescein diacetate (DCFH-DA). H_2O_2 increases the upregulation of ROS induced by propofol, while NAC decreases the upregulation of ROS induced by propofol. (B) H_2O_2 increases the apoptotic capability induced by propofol, whereas NAC decreases the apoptosis induced by propofol. N = 6. *$p < 0.05$, **$p < 0.01$, ***$p < 0.001$.

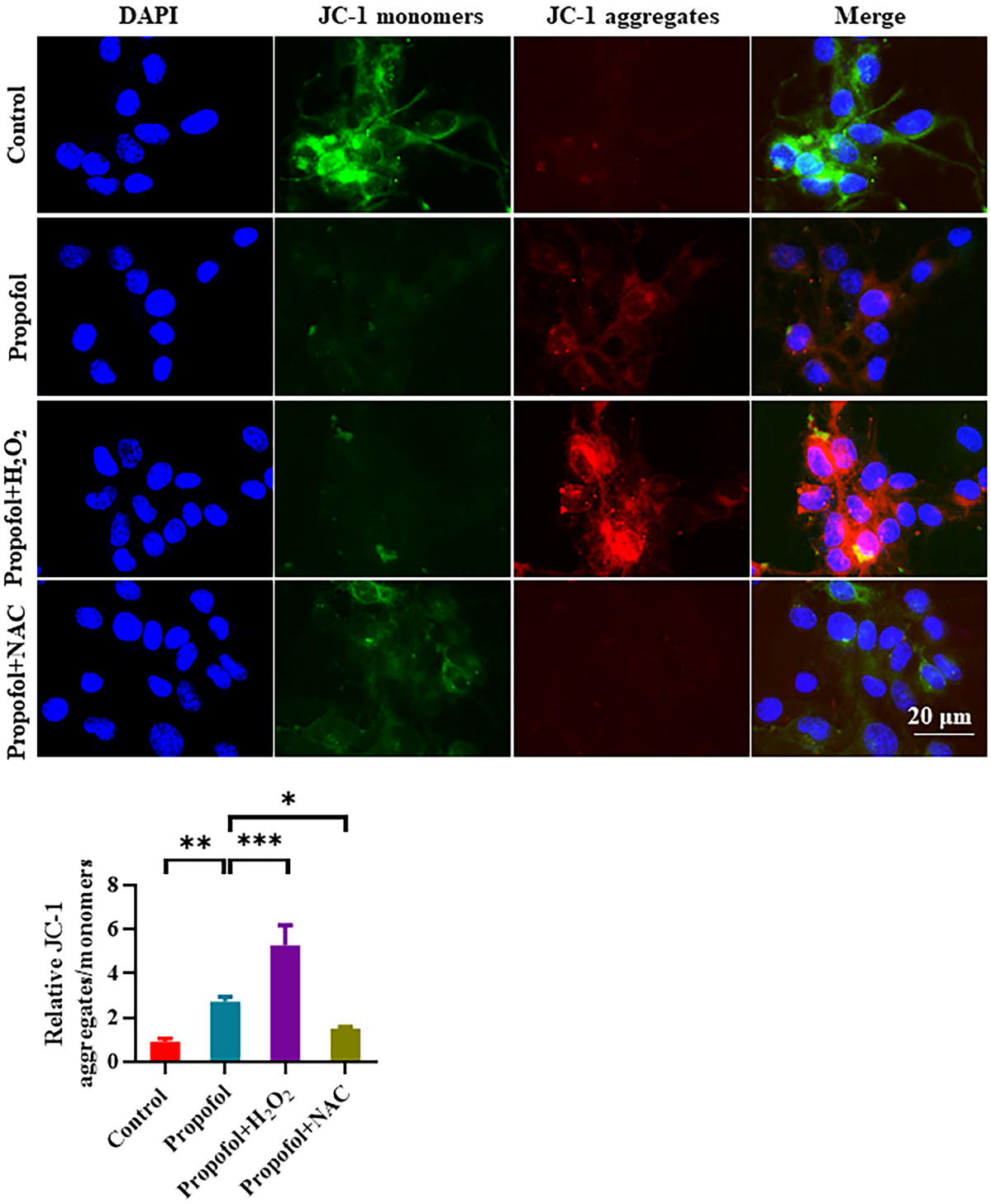

Fig. 4. Mitochondrial membrane potential detected using the JC-1 (5,5′,6,6′-Tetrachloro-1,1′,3,3′-tetraethyl-imidacarbocyanine iodide) assay kit. H_2O_2 increases the mitochondrial membrane potential induced by propofol, while NAC decreases the increase in mitochondrial membrane potential induced by propofol. N = 6. *$p < 0.05$, **$p < 0.01$, ***$p < 0.001$.

neutralizes propofol-induced ROS increase, thus lowering ROS levels and potentially slowing down propofol-induced apoptosis (Fig. 3A).

Subsequently, the influence of propofol on cell death in A549 lung cancer cells was examined through TUNEL staining, with a focus on the role of H_2O_2 and NAC in this process. The propofol-treated group exhibited a significant increase in the number of TUNEL-positive cells compared to the control group ($p < 0.001$), indicating propofol's ability to trigger apoptosis in A549 lung cancer cells. With the addition of hydrogen peroxide to propofol, the number of TUNEL-positive cells continued to rise ($p < 0.001$),

peaking eventually. This suggests that H_2O_2 enhances propofol-induced apoptosis, likely by promoting ROS production and exacerbating cellular oxidative stress. Conversely, the propofol+NAC group had a lower number of TUNEL-positive cells compared to the propofol group ($p < 0.001$), albeit still higher than the control group. This indicates that NAC, acting as an antioxidant, partially neutralizes propofol-induced ROS increase, thereby mitigating apoptosis (Fig. 3B).

Propofol Therapy Enhances Mitochondrial Membrane Potential in Lung Carcinoma Cells

The study assessed alterations in the mitochondrial membrane potential of A549 lung cancer cells under various treatment conditions using the JC-1 assay kit (J8030, Solarbio, Beijing, China). The propofol-treated group exhibited a higher mitochondrial membrane potential compared to the control group ($p < 0.01$), suggesting that propofol may influence mitochondrial function by activating the mitochondrial apoptosis pathway and increasing ROS production, ultimately leading to apoptosis in lung cancer cells. Upon addition of H_2O_2 to propofol, the mitochondrial membrane potential further increased ($p < 0.001$), reaching its peak level. This indicates that H_2O_2 enhances the changes in mitochondrial function induced by propofol, likely by further elevating ROS production, exacerbating cellular oxidative stress, and promoting apoptosis. In comparison to the propofol group, the mitochondrial membrane potential in the propofol+NAC group decreased ($p < 0.05$) but remained higher than in the control group. This suggests that NAC, functioning as an antioxidant, can partially counteract the increase in ROS induced by propofol, thereby mitigating the impact on mitochondrial function and slowing down the apoptosis process (Fig. 4).

Propofol Induces Apoptosis by Upregulating PANX1

The impact of propofol and its combination with hydrogen peroxide or N-acetylcysteine on the levels of PANX1, Bax, Bcl-2, caspase-3, and Cytochrome C proteins in A549 lung cancer cells was assessed via Western blot analysis. In the propofol-treated group, there was a significant increase in the expression level of PANX1 protein ($p < 0.01$), and in the propofol+ H_2O_2 group ($p < 0.001$), this expression level was further elevated. This suggests that propofol can induce apoptosis by upregulating PANX1. The addition of NAC (propofol+NAC group) normalized PANX1 expression to levels similar to those of the control group ($p < 0.001$), indicating that NAC's antioxidant properties can mitigate propofol's impact.

Similarly, the expression of Bax was upregulated in the propofol-treated group ($p < 0.05$) and further enhanced in the propofol+H_2O_2 group ($p < 0.01$), mirroring the changes observed in PANX1. Conversely, the expression of Bcl-2 exhibited an opposite trend, indicating that propofol promotes apoptosis by modulating the Bax/Bcl-2 balance. NAC supplementation led to the restoration of Bax and Bcl-2 expression levels, approaching those seen in the control group.

Patterns of expression for Cleaved caspase-3 and Cytochrome C, both indicative of apoptosis, paralleled those of PANX1 and Bax, showing a notable increase in the propofol ($p < 0.05$) and propofol+H_2O_2 groups ($p < 0.05$). This suggests that propofol triggers apoptosis by activating the apoptotic pathway. The addition of NAC counteracted this effect, restoring protein expression levels to baseline ($p < 0.01$) (Fig. 5).

Inhibition of PANX1 Reduces Propofol-Induced Apoptosis

Transfection with siRNA targeting *PANX1* effectively reduced PANX1 protein levels in the si*PANX1* group ($p < 0.001$), as demonstrated by Western blot (Fig. 6A). Propofol was observed to significantly impede the proliferation of lung cancer cells by diminishing their proliferation capacity ($p < 0.001$), with si*PANX1* partially attenuating this effect ($p < 0.05$). This suggests that *PANX1* plays a pivotal role in propofol-induced inhibition of cell proliferation (Fig. 6B). Fig. 6C showcased that propofol effectively heightened apoptosis in lung cancer cells ($p < 0.001$), while si*PANX1* hindered this effect, thereby reinforcing the involvement of *PANX1* in propofol-induced apoptosis ($p < 0.01$). The assessment of cellular ROS fluorescence intensity revealed that propofol treatment notably escalated ROS levels within lung cancer cells ($p < 0.001$), whereas the inhibition of *PANX1* (si*PANX1*) decreased ROS production, underscoring the significant role of *PANX1* in propofol-induced ROS elevation ($p < 0.001$) (Fig. 6D).

Discussion

This research delved into the impact of propofol on A549 lung cancer cells, specifically examining its role in triggering cell death through the upregulation of PANX1, activation of the mitochondrial apoptosis pathway, and elevation of ROS levels. Our study findings demonstrate that propofol effectively diminishes the survival of lung cancer cells, heightens intracellular ROS levels, and induces apoptosis. These discoveries provide a novel theoretical basis for the potential utilization of propofol in lung cancer therapy.

PANX1, functioning as a protein channel across cell membranes, plays a crucial role in various biological and disease-related processes such as cell death, immune reactions, and cancer progression [25–27]. Our study found that propofol significantly upregulates the expression of PANX1, aligning with previous research findings. This suggests that propofol may induce apoptosis in lung cancer cells by upregulating PANX1, which could represent a crucial mechanism. Furthermore, our research revealed that propofol administration notably increases intracellular

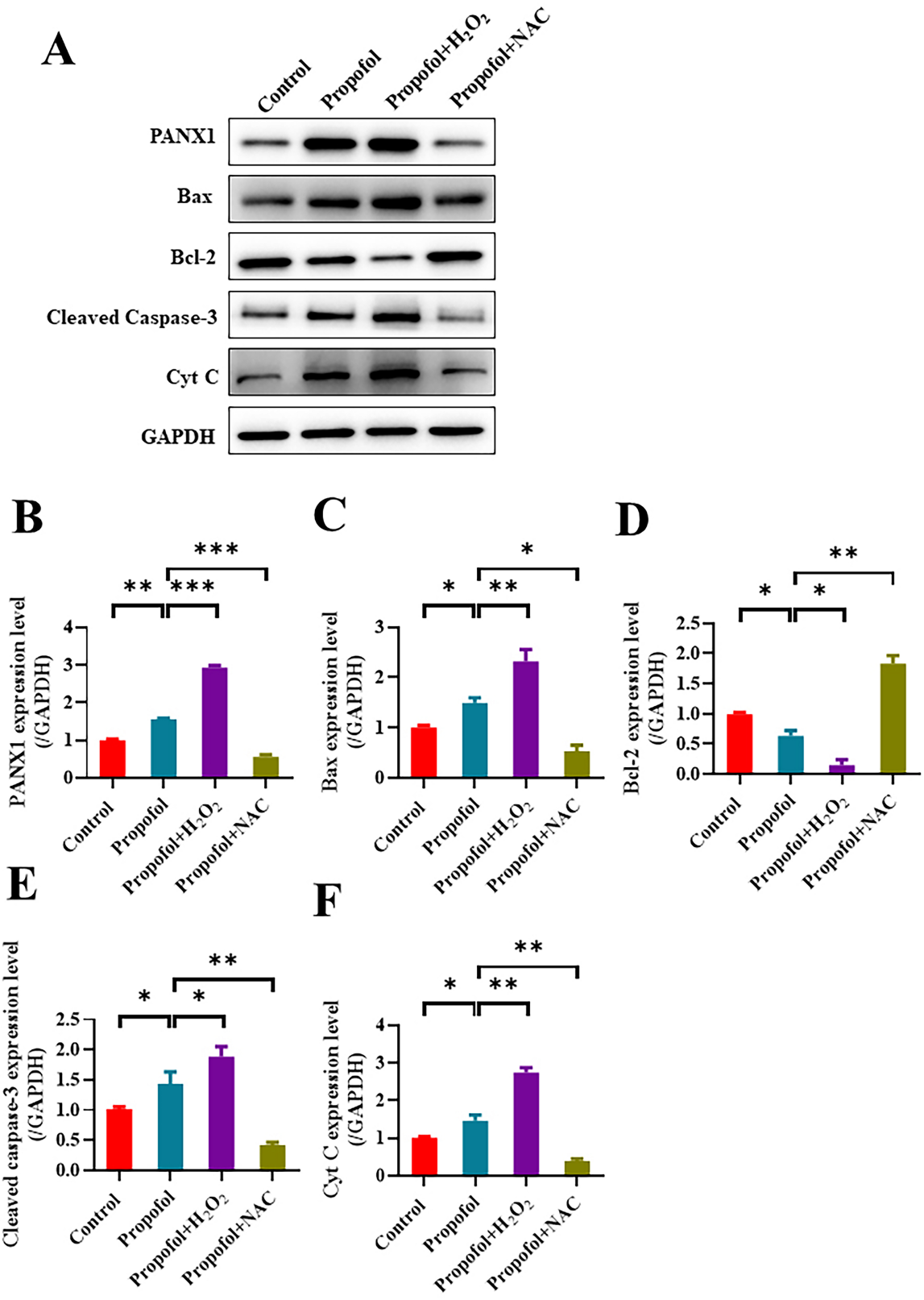

Fig. 5. Propofol induces apoptosis through the upregulation of Pannexin 1 (PANX1). (A) Levels of PANX1, B-cell lymphoma 2 (Bcl-2), Bcl-2-associated X protein (Bax), caspase-3, and Cytochrome C (Cyt C) proteins in A549 cells detected by Western blot. (B–F) Statistical analysis of the expression levels of PANX1 (B), Bax (C), Bcl-2 (D), Cleaved caspase-3 (E), and Cyt C (F) proteins in A549 cells. N = 6. *$p < 0.05$, **$p < 0.01$, ***$p < 0.001$. GAPDH, Glyceraldehyde 3-phosphate dehydrogenase.

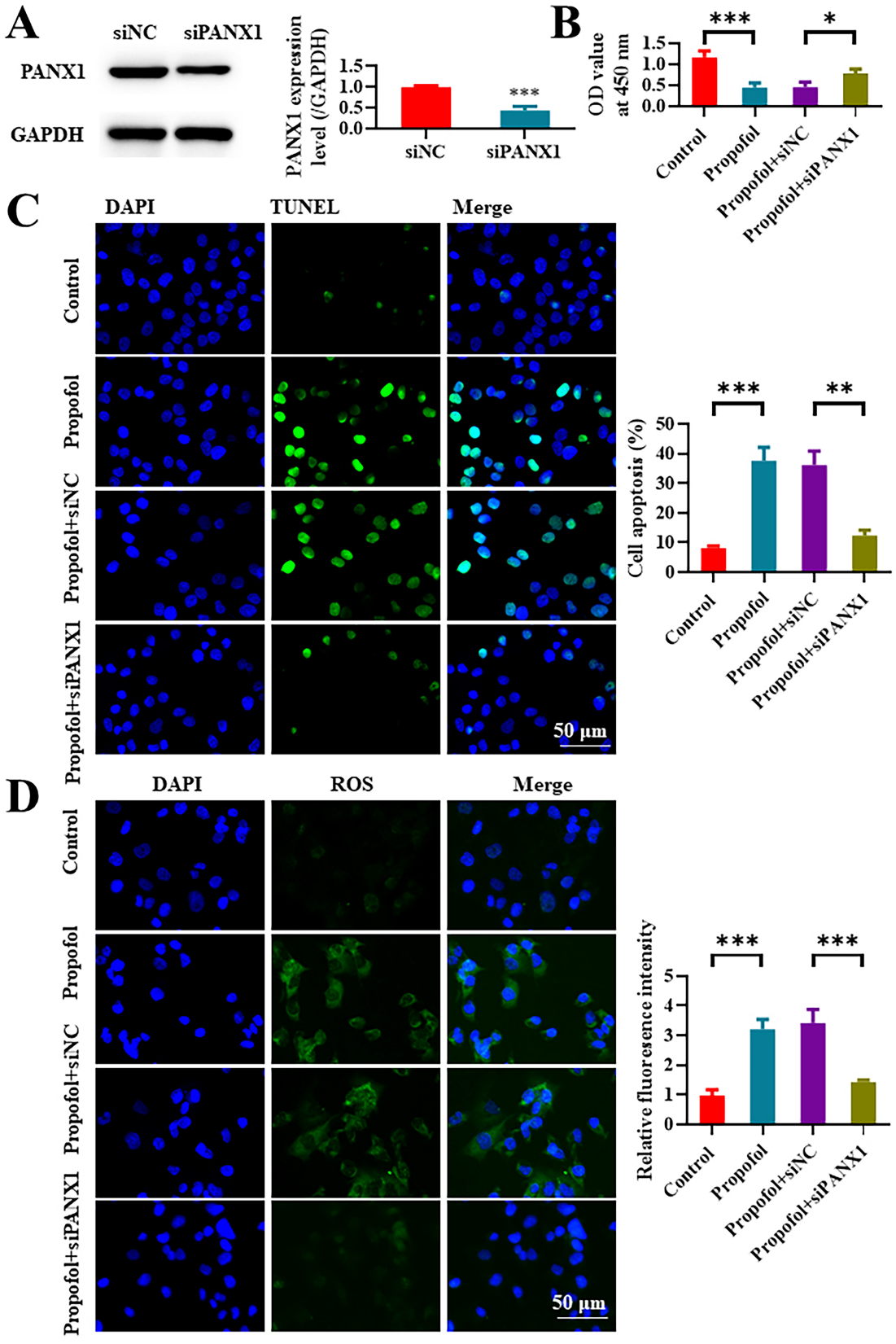

Fig. 6. Inhibition of PANX1 reduces the apoptosis induced by propofol. (A) Western blot detection of si*PANX1* transfection efficiency. (B) Cell proliferation in different treatment groups assessed by Cell Counting Kit-8 (CCK-8) assay. (C) Apoptosis in different treatment groups evaluated by Terminal deoxynucleotidyl transferase dUTP Nick End Labeling (TUNEL) assay. (D) ROS content in different treatment groups detected by DCFH-DA assay. N = 6. *$p < 0.05$, **$p < 0.01$, ***$p < 0.001$. NC, Negative control.

ROS levels, indicating that the elevation in ROS could be another critical factor in propofol-induced apoptosis in lung cancer cells [24,28]. Our study also discovered that propofol has the potential to trigger apoptosis in lung cancer cells by enhancing mitochondrial membrane potential, signifying the activation of the mitochondrial apoptosis pathway, a pivotal pathway in apoptosis [29]. Additionally, through the examination of apoptosis-related protein expression, we further validated that propofol activates the mitochondrial apoptosis pathway. Interestingly, we found that pretreatment with H_2O_2 enhances the inhibitory effect of propofol, while pretreatment with NAC reduces it. These findings suggest that ROS significantly influences the apoptosis triggered by propofol in lung cancer cells. Moreover, when PANX1 expression was inhibited, the apoptotic impact of propofol was notably reduced, providing additional evidence of PANX1's significance in propofol-triggered apoptosis in lung cancer cells.

This research represents the initial effort to elucidate how propofol initiates cell death in lung cancer cells by augmenting PANX1 expression, activating the mitochondrial cell death pathway, and increasing ROS levels. These findings advance our comprehension of propofol's anti-tumor properties and provide novel insights into lung cancer treatment strategies. Specifically, we demonstrated the pivotal role of PANX1 in propofol-triggered cell death in lung cancer cells, laying the foundation for potential anti-cancer approaches targeting PANX1. Furthermore, our study underscores the significance of the mitochondrial apoptosis pathway in propofol-induced apoptosis, offering a fresh perspective on understanding propofol's anti-tumor mechanism.

Although our study sheds light on the involvement of PANX1 in propofol-induced apoptosis in lung cancer cells, further research is warranted to fully elucidate the specific mechanisms of PANX1. Given the complex nature and heterogeneity of lung cancer, it is imperative for future studies to explore potential variations in propofol's effects on different types of lung cancer cells, as well as any potential synergistic or antagonistic effects when combined with other anti-tumor medications.

Based on existing literature and preliminary data, we propose a hypothesis that propofol might modulate PANX1 expression through transcriptional regulation or post-transcriptional modifications, rather than directly impacting protein translation or degradation processes. It is plausible that propofol's effects on transcription factors or signaling pathways associated with PANX1 regulation, such as hypoxia-inducible factor 1-alpha (HIF-1α), nuclear factor-kappa B (NF-κB), or mitogen-activated protein kinase (MAPK) pathways, could be involved. Further exploration into these potential mechanisms is warranted.

Future investigations employing techniques such as chromatin immunoprecipitation (ChIP) assays, luciferase reporter assays, and RNA sequencing (RNA-seq) analysis hold promise for unraveling the precise transcriptional regulatory mechanisms responsible for propofol-induced PANX1 upregulation. Furthermore, exploring the roles of microRNAs or epigenetic modifications in mediating PANX1 expression changes following propofol treatment could offer valuable insights into this process, thereby enhancing our understanding of propofol's effects on PANX1 expression.

Conclusion

This study elucidates a novel mechanism by which propofol induces cell death in lung cancer cells, highlighting the critical role of PANX1 upregulation, mitochondrial apoptosis pathway activation, and ROS elevation. This discovery provides both theoretical support and empirical evidence for the potential therapeutic use of propofol in treating lung cancer. Further investigations are warranted to delve into the specific mechanisms of propofol action in various tumor types and its potential synergistic effects when combined with other anti-cancer medications. Such studies aim to strengthen the scientific foundation for propofol's clinical application in cancer therapy.

Availability of Data and Materials

The corresponding author will provide the data that underpin the study's conclusions with a reasonable application.

Author Contributions

JZ and YGS designed the study; all authors conducted the study; AQC collected and analyzed the data; YGS participated in drafting the manuscript, and all authors contributed to critical revision of the manuscript for important intellectual content. All authors gave final approval of the version to be published. All authors participated fully in the work, took public responsibility for appropriate portions of the content, and agreed to be accountable for all aspects of the work in ensuring that questions related to the accuracy or completeness of any part of the work are appropriately investigated and resolved.

Ethics Approval and Consent to Participate

Not applicable.

Acknowledgment

Not applicable.

Funding

This research received no external funding.

Conflict of Interest

The authors declare no conflict of interest.

References

[1] Rudin CM, Brambilla E, Faivre-Finn C, Sage J. Small-cell lung cancer. Nature Reviews. Disease Primers. 2021; 7: 3.

[2] Howlader N, Forjaz G, Mooradian MJ, Meza R, Kong CY, Cronin KA, *et al*. The Effect of Advances in Lung-Cancer Treatment on Population Mortality. The New England Journal of Medicine. 2020; 383: 640–649.

[3] Iams WT, Porter J, Horn L. Immunotherapeutic approaches for small-cell lung cancer. Nature Reviews. Clinical Oncology. 2020; 17: 300–312.

[4] Leiter A, Veluswamy RR, Wisnivesky JP. The global burden of lung cancer: current status and future trends. Nature Reviews. Clinical Oncology. 2023; 20: 624–639.

[5] Yang D, Liu Y, Bai C, Wang X, Powell CA. Epidemiology of lung cancer and lung cancer screening programs in China and the United States. Cancer Letters. 2020; 468: 82–87.

[6] Oudkerk M, Liu S, Heuvelmans MA, Walter JE, Field JK. Lung cancer LDCT screening and mortality reduction - evidence, pitfalls and future perspectives. Nature Reviews. Clinical Oncology. 2021; 18: 135–151.

[7] Wang M, Herbst RS, Boshoff C. Toward personalized treatment approaches for non-small-cell lung cancer. Nature Medicine. 2021; 27: 1345–1356.

[8] Onoi K, Chihara Y, Uchino J, Shimamoto T, Morimoto Y, Iwasaku M, *et al*. Immune Checkpoint Inhibitors for Lung Cancer Treatment: A Review. Journal of Clinical Medicine. 2020; 9: 1362.

[9] Nooreldeen R, Bach H. Current and Future Development in Lung Cancer Diagnosis. International Journal of Molecular Sciences. 2021; 22: 8661.

[10] Li Y, Yan B, He S. Advances and challenges in the treatment of lung cancer. Biomedicine & Pharmacotherapy. 2023; 169: 115891.

[11] Bao L, Sun K, Zhang X. PANX1 is a potential prognostic biomarker associated with immune infiltration in pancreatic adenocarcinoma: A pan-cancer analysis. Channels (Austin, Tex.). 2021; 15: 680–696.

[12] Huang KCY, Chiang SF, Lin PC, Hong WZ, Yang PC, Chang HP, *et al*. TNFα modulates PANX1 activation to promote ATP release and enhance P2RX7-mediated antitumor immune responses after chemotherapy in colorectal cancer. Cell Death & Disease. 2024; 15: 24.

[13] Long W, Zhang H, Xie H, Wang Y, Zhang L, Yu H, *et al*. Panx1 Promotes Cisplatin-induced Apoptosis of A549 Cells by Regulating ATP/IP3 Pathway. Cancer Research on Prevention and Treatment. 2021; 48: 674–678.

[14] Imamura H, Sakamoto S, Yoshida T, Matsui Y, Penuela S, Laird DW, *et al*. Single-cell dynamics of pannexin-1-facilitated programmed ATP loss during apoptosis. eLife. 2020; 9: e61960.

[15] Ying W, Zheng K, Wu Y, Wang O. Pannexin 1 Mediates Gastric Cancer Cell Epithelial-Mesenchymal Transition via Aquaporin 5. Biological & Pharmaceutical Bulletin. 2021; 44: 1111–1119.

[16] Davidson SM, Adameová A, Barile L, Cabrera-Fuentes HA, Lazou A, Pagliaro P, *et al*. Mitochondrial and mitochondrial-independent pathways of myocardial cell death during ischaemia and reperfusion injury. Journal of Cellular and Molecular Medicine. 2020; 24: 3795–3806.

[17] Bock FJ, Tait SWG. Mitochondria as multifaceted regulators of cell death. Nature Reviews. Molecular Cell Biology. 2020; 21: 85–100.

[18] Chipuk JE, Mohammed JN, Gelles JD, Chen Y. Mechanistic connections between mitochondrial biology and regulated cell death. Developmental Cell. 2021; 56: 1221–1233.

[19] Bauer TM, Murphy E. Role of Mitochondrial Calcium and the Permeability Transition Pore in Regulating Cell Death. Circulation Research. 2020; 126: 280–293.

[20] Zhang K, Zhou X, Wang J, Zhou Y, Qi W, Chen H, *et al*. Dendrobium officinale polysaccharide triggers mitochondrial disorder to induce colon cancer cell death via ROS-AMPK-autophagy pathway. Carbohydrate Polymers. 2021; 264: 118018.

[21] Gao X, Mi Y, Guo N, Luan J, Xu H, Hu Z, *et al*. The mechanism of propofol in cancer development: An updated review. Asia-Pacific Journal of Clinical Oncology. 2020; 16: e3–e11.

[22] Yu B, Gao W, Zhou H, Miao X, Chang Y, Wang L, *et al*. Propofol induces apoptosis of breast cancer cells by downregulation of miR-24 signal pathway. Cancer Biomarkers: Section a of Disease Markers. 2018; 21: 513–519.

[23] Jiang S, Liu Y, Huang L, Zhang F, Kang R. Effects of propofol on cancer development and chemotherapy: Potential mechanisms. European Journal of Pharmacology. 2018; 831: 46–51.

[24] Wang H, Zhao L, Wu J, Hong J, Wang S. Propofol induces ROS-mediated intrinsic apoptosis and migration in triple-negative breast cancer cells. Oncology Letters. 2020; 20: 810–816.

[25] Dahl G. The Pannexin1 membrane channel: distinct conformations and functions. FEBS Letters. 2018; 592: 3201–3209.

[26] Bhat EA, Sajjad N. Human Pannexin 1 channel: Insight in structure-function mechanism and its potential physiological roles. Molecular and Cellular Biochemistry. 2021; 476: 1529–1540.

[27] Whyte-Fagundes P, Zoidl G. Mechanisms of pannexin1 channel gating and regulation. Biochimica et Biophysica Acta. Biomembranes. 2018; 1860: 65–71.

[28] Sun C, Liu P, Pei L, Zhao M, Huang Y. Propofol Inhibits Proliferation and Augments the Anti-Tumor Effect of Doxorubicin and Paclitaxel Partly Through Promoting Ferroptosis in Triple-Negative Breast Cancer Cells. Frontiers in Oncology. 2022; 12: 837974.

[29] Sumi C, Okamoto A, Tanaka H, Nishi K, Kusunoki M, Shoji T, *et al*. Propofol induces a metabolic switch to glycolysis and cell death in a mitochondrial electron transport chain-dependent manner. PloS One. 2018; 13: e0192796.